ACS APPLIED POLYMER MATERIALS

pubs.acs.org/acsapm Article

Device for the Acquisition of Dynamic Data Enables the Rapid Characterization of Polymer Membranes

Zachary W. Muetzel, Jonathan Aubuchon Ouimet, and William A. Phillip*

Cite This: ACS Appl. Polym. Mater. 2022, 4, 3438−3447 Read Online

ACCESS | Metrics & More | Article Recommendations | Supporting Information

ABSTRACT: Creating systems and techniques capable of reducing the time, energy, and resources needed to characterize the transport properties of polymer membranes can help to increase the rate of material and process development. Within this study, commercially available hardware and 3D-printed parts are integrated with a graphical user interface to develop an apparatus that automates the characterization of membrane transport properties. The system synchronizes the collection of the mass, concentration, and pressure data required to determine the hydraulic permeability and solute permeability coefficients. Automating the data collection and shutdown processes removes the need for a researcher to be present after the start of the experiment, effectively reducing the demand on their time by 40% per experiment. Moreover, the experiments generate more information than standard approaches by identifying the concentration dependencies of the transport coefficients. As an example, diafiltration experiments executed using the acquisition of dynamic data (ADD) device quantified $MgCl_2$ rejection by charge-functionalized poly[trifluoroethyl methacrylate-*co*-oligo(ethylene glycol) methyl ether methacrylate-*co*-glycidyl methacrylate] membranes over a range of retentate concentrations from 5 to 65 mM $MgCl_2$. A single diafiltration experiment corroborated previously reported data, collected from a series of one-off filtration experiments, on membranes functionalized with hexamethylene diamine moieties. Membranes functionalized with ethylene diamine and trimethylolpropane tris[poly(propylene glycol), amine terminated] ether were also analyzed. High-throughput diafiltration experiments were able to elucidate the distinct concentration-dependent rejection profiles that resulted from these changes to the membrane chemistry. The versatility of the ADD device was highlighted by adapting it to characterize membrane sorbents using constant volumetric flux breakthrough experiments. Ultimately, the ability of this device to characterize functional polymer membranes will aid in the development of fundamental insights that connect macroscopic membrane properties with macromolecular design.

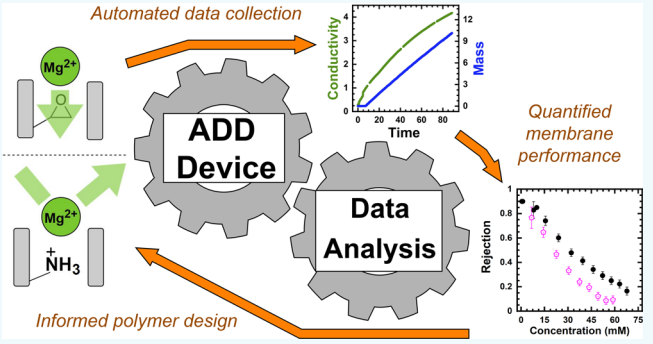

KEYWORDS: *diafiltration, high-throughput characterization, data acquisition, membranes, breakthrough experiments, adsorbents*

1. INTRODUCTION

Membranes separate mixtures by modulating the relative fluxes of the component species. The differences in flux can be based on variations in a number of physio-chemical descriptors (e.g., size, charge, or solubility). For instance, a porous polymer membrane can retain a solute whose size is larger than its characteristic pore size, while the transport of a second species, whose size is much smaller than the pore size, is unhindered. Here, the separation occurs because the flux of the larger species is restricted to zero, while that of the smaller species remains finite. Advances in polymer science and engineering have led to the development of membranes capable of executing even more challenging separations, and as a result, membrane-based separations have helped to transform several of the processes which modern society relies upon (e.g., the processing of food,[1] the purification of therapeutic drugs,[2−7] gas separations,[8−10] and supplementing potable water resources[11−14]). However, the need for selective separations persists and generating the information needed to molecularly engineer polymer membranes for emerging processes will require rigorously quantifying material fluxes.

The flux through a membrane, J, is proportional to a driving force, ∇F (e.g., a gradient in chemical or mechanical potential).[15]

$$J \propto \nabla F \tag{1}$$

Received: January 9, 2022
Accepted: April 6, 2022
Published: April 20, 2022

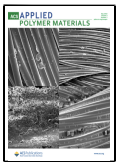

Because the gradient occurs over a thin dimension, that is, the thickness of the membrane, it is often approximated using a difference. For example, eq 2 relates the volumetric flux of water to the applied pressure difference across the membrane, ΔP, using the hydraulic permeability coefficient, L_p.[16] In a similar manner, the molar flux of the solute is proportional to the transmembrane concentration difference, Δc, through the solute permeability coefficient, B (eq 3).[16]

$$J_w = L_p \Delta P \tag{2}$$

$$J_s = B \Delta c \tag{3}$$

Alternatively, expressions similar to eqs 2 and 3 can be derived by integrating the differential equations governing transport over the membrane thickness. Regardless of the approach utilized, the values of L_p and B are determined by factors such as the dominant transport mechanisms, the nature of the permeating specie(s), and the nanostructure and chemistry of the membrane. Therefore, examining the dependencies of L_p and B in the context of other structural and chemical analysis can inform the relationships needed to design next generation polymer membranes. For example, while B for some membranes is independent of the solute concentration,[17] other membranes (e.g., charge-functionalized membranes) exhibit concentration-dependent B values.[18,19] Quantifying these dependencies can help identify underlying transport mechanisms and accelerate material development.[20]

The creation of techniques capable of reducing the time and resources necessary to quantify material fluxes over a range of operational conditions would aid efforts to elucidate the relevant dependencies of permeability coefficients. For instance, Ghosh et al. developed a pulsed sample injection technique to accelerate the optimization of protein separations.[21,22] The technique was equipped to identify how the pH and ionic strength-dependent conformations and surface charges of proteins influenced their transport through ultrafiltration membranes. Quantifying transport coefficients subject to systematic variations in pH and salt concentration shed light on the operating conditions that enhanced the filtration of proteins from contaminants. The need for methodologies, such as that developed by Ghosh et al., is particularly relevant given the growing interest in polymer membranes with solute-tailored selectivity. These membranes, which are designed to isolate one solute from a complex mixture, often rely on grafting chelating or coordinating groups within the pores of a membrane. However, little is known about the fundamental structure−function relationships for these membranes with bound carriers that facilitate solute transport. Moreover, the composition of the feed stream encountered by these membranes can impact material fluxes. For example, attractive interactions between two dissolved species can increase the complexity of and the resources necessary to achieve a separation.[5] Alternatively, repulsive interactions can cause the presence of one dissolved solute to increase the flux of another solute.[23−25] As such, model polymer membranes, which allow for systematic variations in nanostructure and pore wall chemistry, combined with techniques that quickly characterize permeability coefficients as a function of solution composition can be leveraged to elucidate the underlying mechanisms and molecular design principles that promote the selective transport of solutes.

In this study, commercially available hardware and software are used to design and construct an automated device that rapidly characterizes the transport parameters of membranes as a function of solution properties. The sample collection and experimental shutdown processes are automated through the use of a programmable motor and valves and 3D-printed parts. A versatile graphical user interface (GUI) provides the experimenter with control over the types of data recorded and the number of samples that will be collected. After samples are analyzed, post processing of the results using a standardized file format streamlines data analysis. The implications of the acquisition of dynamic data (ADD) device for accelerating material development are examined using a series of diafiltration and breakthrough experiments. Specifically, the diafiltration experiments examine the concentration-dependent transport parameters of charge-functionalized copolymer membranes that remove dissolved ions through electrostatic interactions. The breakthrough experiments, which exemplify the versatility of the system, are used to characterize the performance of an adsorbent membrane designed for the selective capture of transition metal ions. This information related to functional polymer materials can inform the molecular design of next-generation membranes for water treatment,[11,26] the electronics industry,[27,28] and biopharmaceutical applications.[7]

2. PHYSICAL CONCEPT FOR THE ADD DEVICE

2.1. Materials. All experiments characterizing charge-functionalized copolymer membranes were conducted using a 10 mL Amicon 8010 stirred cell (Amicon, Burlington, Massachusetts). Mass data were collected with an OHAUS adventure series balance (OHAUS, Parsippany, New Jersey). Pressure data were collected using an Omega PX409 USBH pressure transducer (Omega, Norwalk, Connecticut). A CN0359 conductivity measurement board (Analog Devices Incorporated, Thief River Falls, Minnesota) generated a square wave AC current to maintain a constant voltage differential of 0.7 V across the two inner electrodes of an LFS 1107 conductivity probe (Innovative Sensor Technology, Las Vegas, Nevada). Initially, the conductivity probe and measurement board were not able to generate a stable conductivity reading. This issue, which was addressed by modifying the circuitry as outlined in the Supporting Information, was attributed to a small nonzero DC component of the current in the excitation signal. The leads of the probe were soldered to 32-gauge space-saver wire (McMaster Carr, Elmhurst, Illinois) and potted with PT328 epoxy (Permabond, Pottstown, Pennsylvania) to protect the leads from saline solutions. The CN0359 conductivity board is powered by an AC 100−240 V to DC 12 V transformer wall adapter (Mouser Electronics, Mansfield, Texas). An industrial USB to RS485 converter adapter (Waveshare, Guangdong Province, China) was used to connect the CN0359 conductivity measurement board to the USB hub. The OHAUS balance and PX409 pressure transducer were connected to the USB hub through a USB-A cable. All data were transmitted to a computer where it was displayed and stored using an in-house MATLAB code.

Two 1/4″ 12 V DC Stainless Electric Solenoid Valves (electricsolenoidvalves.com, Hoffman Lane Islandia, New York) were used to (1) control the main pressure line and (2) to act as a pressure relief valve. The solenoid valves were controlled by a KinCony Smart Switch 4 gang ethernet relay module (KinCony, Zhejiang Province, China), which was connected to the USB hub using a USB to RS232 Adapter with

https://doi.org/10.1021/acsapm.2c00048
ACS Appl. Polym. Mater. 2022, 4, 3438−3447

PL2303 chipset, USB 2.0 male to RS232 male D89 serial converter cable (CableCreation, China).

A Lynxmotion (LSS)—adapter board (USB Mini) (RobotShop, Mirabel, Canada) was used to control a Lynxmotion Smart Servo (LSS)—Standard (ST1) motor (RobotShop, Mirabel, Canada). The adapter board was powered via an AC to DC power adapter 12 V 3A XT60 wall plug (Crazepony, Guangdong Province, China). The Lynxmotion adapter board was connected to a 7-Port USB 3.0 hub using a UGREEN Mini USB cable, A-Male to Mini B cord USB 2.0 (UGREEN, Guangdong Province, China). If not listed here explicitly, all other connections were provided with the equipment listed above.

2.2. 3D-Printed Materials. All 3D-printed parts were made in-house using polylactic acid or acrylonitrile−butadiene−styrene filament. Designs were created using SOLIDWORKS 3D CAD software (Dassault Systèmes, Vélizy-Villacoublay, France). Boxes with removable covers were used to house and protect the CN0359 conductivity board and Lynxmotion adapter board from water. A motor anchor was printed to secure the Lynxmotion motor to the OHAUS balance. Two important components of the motor anchor must be accurately printed to ensure a tight fit between the motor and balance. The motor anchor legs were printed with dimensions of 144.8 mm × 113 mm to fit the balance of dimensions 146 mm × 114.3 mm. The motor anchor legs were printed smaller than the balance to allow for fine tuning (i.e., sanding) of the leg dimensions during post-processing. Next, the capsule that houses the motor was printed with dimensions of 51.6 mm × 26.2 mm to hold the 50.8 mm × 25.4 mm motor. Permeate vial holders were designed to hold various-sized scintillation vials. The permeate vial holders were attached to the Lynxmotion motor with screws. An evaporation control cover was printed to limit evaporative water loss during experiments. The .stl files for all parts can be accessed using a link included within the Supporting Information.

3. RESULTS AND DISCUSSION

3.1. Commercially Available Hardware Automates Membrane Characterization. The ADD device automates the collection of several data types needed to quantify membrane transport parameters. To begin, Figure 1 shows that a pressure transducer, located immediately after a pressurized supply of nitrogen, measures the system pressure and a balance records the permeate mass as a function of time. For pure solvent systems, this knowledge of the operating pressure and the mass permeation rate enables the determination of the hydraulic permeability coefficient. For feed solutions containing dissolved solutes, the water flux equation is updated to account for the influence of the osmotic pressure difference across the membrane, $\Delta\Pi$.

$$J_w = L_p(\Delta P - \sigma\Delta\Pi) \quad (4)$$

The fraction of $\Delta\Pi$ exerted is accounted for using the reflection coefficient, σ, whose value depends on the feed solution composition and membrane structure.

The reflection coefficient and solute permeability coefficient are determined by conducting experiments at varied salt concentrations.[17] Consequently, capturing the solute concentration difference across the membrane is required. As shown in Figure 1, the ADD device uses a CN0359 conductivity

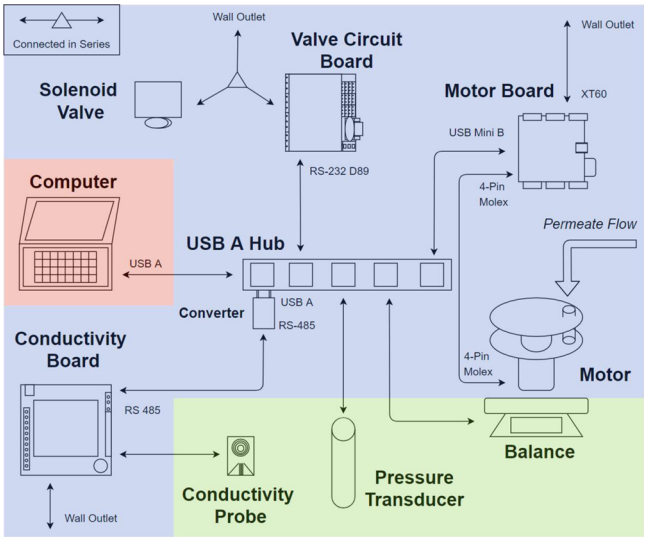

Figure 1. Schematic illustration of the connections between components within the ADD device. Components are separated into three categories: data collection (green), data transfer and device control (blue), and user interface (red). All equipment drew power from either a wall outlet or through the USB serial interface. The CN0359 conductivity board controlled the conductivity probe and transmitted data to the computer through an RS485 to USB adapter. Pressure data, recorded by the PX409 pressure transducer, were transmitted directly to the computer through a USB serial port. Data from the balance were sent to the computer via a RS232 to USB cable. The motor, controlled through the Lynxmotion motor adapter board (motor board), rotated the vials based on user-specified mass values in the ADD GUI (graphical user interface). The ON/OFF states of the solenoid valves were controlled through a KinCony circuit board (valve circuit board). All relevant port types are shown near the arrow of the device they enter or leave.

board and an inline conductivity probe, positioned within the stirred cell (Figure S2d), to obtain measurements of the retentate concentration over the course of the experiment. The conductivity probe is soldered to flexible 32-gauge space saver wires to ensure sufficient room exists to manipulate the wires through the head of the stirred cell and tubing. Additionally, the flexible wiring prevents tears within the plastic sheathing. As these wires are in direct contact with the salt solution, a tear in this sheath can form a salt bridge between the two wires and short the probe. To monitor the experimental retentate conditions, the CN0359 conductivity board supplies a square wave AC current to maintain a 0.7 V differential across the sensing electrodes of the conductivity probe. The data are recorded by the computer.

The permeate solution can be analyzed after the experiment concludes to determine the ion concentration and establish the concentration difference across the membrane. This experimental design requires a new scintillation vial be placed under the permeate drip line at user-specified intervals. A circular scintillation vial holder screwed to the top of a programmable servo motor automates the vial swaps. Figure 1 illustrates that the motor is controlled through a Lynxmotion Motor Board. As solution permeates through the membrane, the weight recorded by the balance increases. The motor operates in a feedback loop and rotates individual vials under the permeate drip line upon reaching user-specified intervals (e.g., 1 g). Theoretically, the maximum permeate flow rate that can be measured is determined by the maximum speed (revolutions

https://doi.org/10.1021/acsapm.2c00048
ACS Appl. Polym. Mater. 2022, 4, 3438−3447

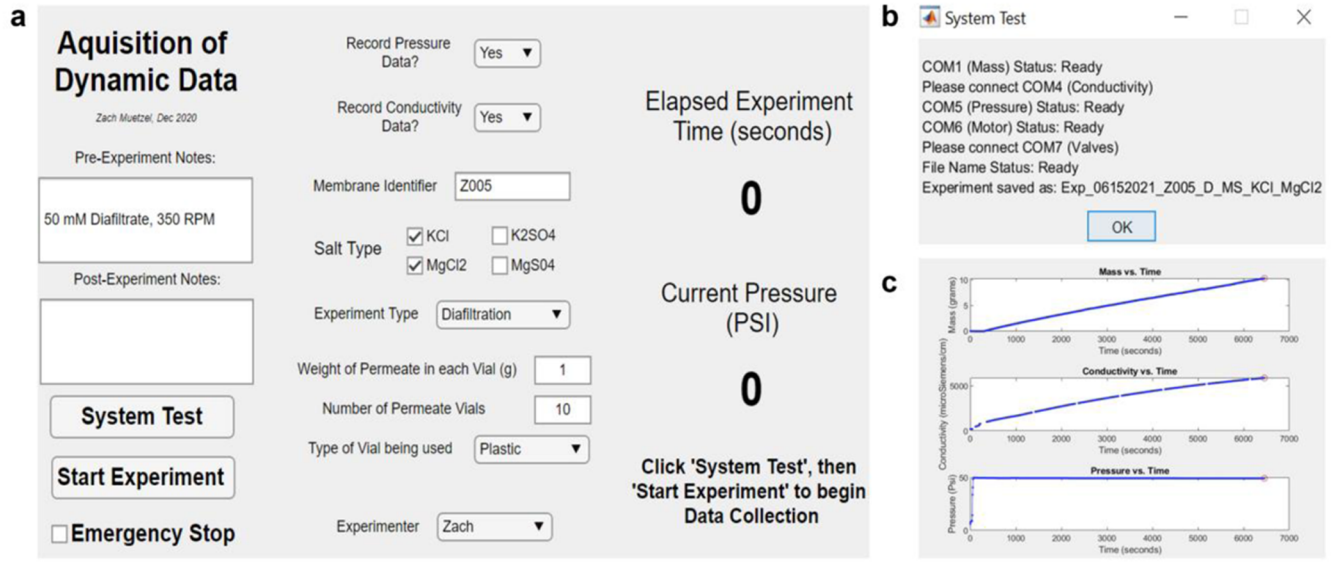

Figure 2. (a) ADD GUI is used to specify the experimental conditions (e.g., salt type, membrane identifier, and experiment type) and begin data collection. The "System Test" button ensures that the system is properly communicating with each one of the data collection components. Additionally, within the System Test, the ADD device commands the motor to rotate through each of the vial positions once, completing a full rotation. (b) System feedback is provided before executing an experiment. In this example, the user is informed that the solenoid pressure valves and conductivity board are not communicating with the system. All devices should show a "Ready" status before a successful experiment can be executed. The ADD device automatically saves collected data and shuts down the system at the end of the experiment. The "Emergency Stop" button stops the experiment in the case that a hazard (e.g., leaks) presents itself. (c) Graphs providing real time data are created during an experiment. The presented graphs represent a full data set captured at the end of an experiment.

per minute) of the Lynxmotion motor. Under the experimental conditions studied, the maximum flow rate that could be accurately captured is 1 mL s^{-1}. The corresponding calculations and assumptions made to determine this value are outlined within the Supporting Information.

Figure S3a displays the circular scintillation vial holder resting on top of the motor. The motor is positioned inside an anchor that is attached to the balance. When the mass of the collected samples reaches the user-specified threshold, the motor will rotate the vial holder clockwise to place the subsequent vial under the permeate outlet (Figure S3b). Once the last permeate vial is filled, if the experiment is using a nitrogen-fed pressure line, the valve circuit board activates two solenoid valves that depressurize the system. The power to the main solenoid valve is cut and the valve closes. Immediately after, power is supplied to the second solenoid valve, which causes it to open and depressurize the system. After 30 s, the system is depressurized and the power to the second solenoid valve is cut off.

During long experiments, evaporation can occur while the collected permeate vials remain exposed, open to ambient conditions. Evaporative loses of the solvent will increase the relative concentration of ions in the permeate vials and can skew results. To mitigate evaporative loses, a lid was designed to cover the permeate vials (Figure S3c). As the motor moves empty vials under the permeate drip line, the hole in the cover permits the permeate to drip into the current vial while keeping the remaining vials covered. Assuming the air immediately above the permeate solution is saturated with water and the room has a relative humidity of 60%, the loss of water is theoretically calculated to be equal to 7.34 μL h^{-1} $vial^{-1}$. Experimentally, a similar rate of 7.52 μL h^{-1} $vial^{-1}$ was determined. The cover shields the vials from ambient conditions and decreases the evaporative losses to an experimentally determined value of 4.99 μL h^{-1} $vial^{-1}$. For most experiments, which take between 2 and 4 h, the amount of water lost in a vial is negligible. For long experiments (e.g., those that lasts 50 h), the first permeate vial can lose up to 0.25 mL of water due to evaporation.

3.2. Software Provides Dependable Data Collection under Various Experimental Conditions. The GUI is used to specify the characteristics of an experiment executed using the ADD device (Figure 2a). Before beginning the experiment, the "System Test" feature is used to confirm the devices are properly connected and all necessary information is entered into the GUI. A window (Figure 2b) provides feedback about the connection status of the devices and confirms that a valid and unique filename can be generated. This ensures that previously collected data sets are not overwritten. Once the user confirms that all the desired devices are connected, "Start Experiment" is selected to begin data collection. Throughout the experiment, the ADD device displays mass, pressure, and conductivity data at 5 s intervals in real time via three updating graphs (Figure 2c). When the final permeate vial is filled, the ADD device automatically ends data collection. The data collected, along with any notes added by the experimenter, are saved under the unique experiment name in an array format as a .txt file. If the experiment is using a nitrogen-fed pressure line, the ADD device will communicate with the valve control board to shut down the experiment, removing the need for the experimenter to be present at the conclusion of the experiment. Further details regarding the GUI are provided within the Supporting Information.

3.3. Automated Diafiltration Requires 40% Less Time. The benefits of the ADD device for material development are exemplified by diafiltration experiments used to characterize the concentration-dependent properties of charge-functionalized poly[trifluoroethyl methacrylate-*co*-

https://doi.org/10.1021/acsapm.2c00048
ACS Appl. Polym. Mater. 2022, 4, 3438−3447

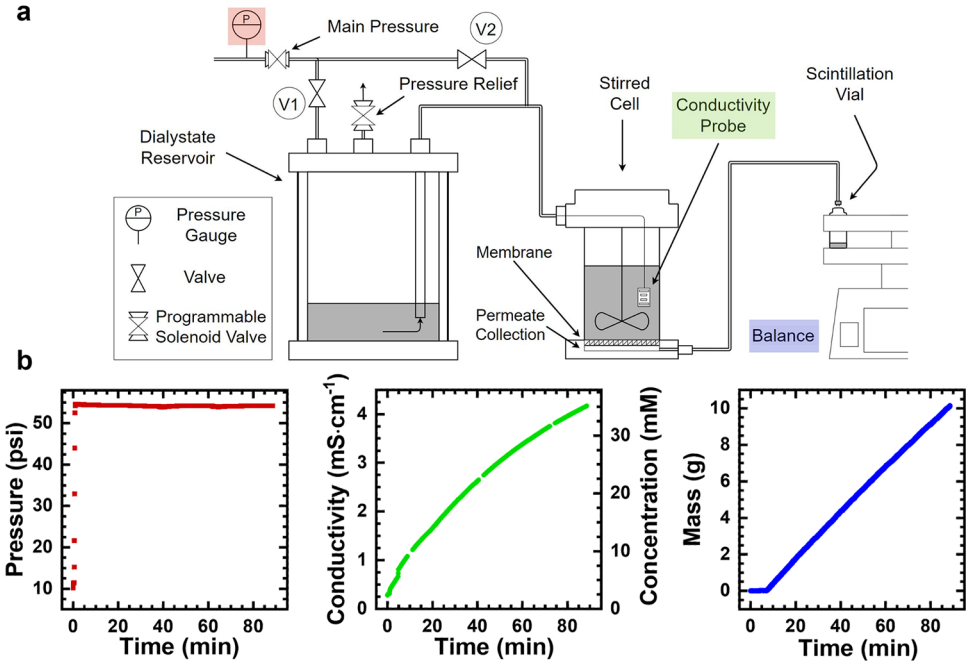

Figure 3. (a) Schematic of the modified diafiltration apparatus. A diafiltrate reservoir holds a high concentration salt solution that is systematically dosed into the stirred cell. The permeate is collected within scintillation vials that rest on top of a balance. The inline conductivity probe measures the real-time conductivity of the solution within the stirred cell. Pressure is supplied by an in-house nitrogen system and controlled by the ADD device using two programmable solenoid valves. The valves allow the ADD device to automatically shut down once the last permeate vial is filled. (b) Graphs of the raw data collected from a diafiltration experiment characterizing a copolymer membrane. The location of each data collecting device is highlighted within the apparatus. The initial low-pressure data points (i.e., 9 psi) correspond to the experiment startup. An operating pressure of 55 psi was used. The conductivity increases as the high concentration diafiltrate is dosed into the stirred cell at a rate equal to the permeate entering the scintillation vial. For the first 8 min of the experiment, the mass measurement remains at zero. This corresponds to the filling of the tube between the stirred cell and the scintillation vial.

oligo(ethylene glycol) methyl ether methacrylate-*co*-glycidyl methacrylate] [P(TFEMA−OEGMA−GMA)] membranes (Figure 3). The synthesis and characterization of the P(TFEMA−OEGMA−GMA) copolymer and the membrane casting process are detailed in prior studies.[29,30] The essential features for the current effort are that due to the self-assembly of the copolymer, membranes with pores 2 nm in diameter and surfaces lined by epoxide rings can be cast from these materials. While the as-cast, parent membranes are not expected to reject dissolved salts well, due to their neutral surface and large pore size relative to hydrated ions, they can be functionalized post-fabrication through epoxide ring opening reactions (Figure 4a). Previously, it was hypothesized that membranes functionalized with hexamethylene diamine rejected dissolved salts through electrostatic repulsion between the charged ammonium moieties and cations. Therefore, four filtration experiments were conducted with $MgCl_2$ feed concentrations ranging from 0.5 to 100 mM.[18] While the experiments did demonstrate a concentration-dependent $MgCl_2$ rejection, they did not fully elucidate the system behavior as it transitioned from a high rejection at 0.5 mM to a low rejection at 100 mM. Here, a series of diafiltration experiments are designed to replicate the prior experiments while also generating more information regarding $MgCl_2$ rejection at the intermediate range of concentrations. Furthermore, the study was expanded to highlight how the ADD device can be used to develop structure−function insights more rapidly and reproducibly. Specifically, parent P(TFEMA−OEGMA−GMA) membranes were functionalized using two additional amine chemistries, ethylene diamine and trimethylolpropane tris[poly(propylene glycol), amine terminated] ether, to examine the influence of the spacer length and chemistry on the transport characteristics of the membranes.

Before each diafiltration experiment, approximately 5 mL of DI water was permeated through the membrane to flush any residual solute from the system. Afterward, the volume above the membrane is filled with 11 mL of 1 mM $MgCl_2$ salt solution. The stirred cell is covered and set on a stir plate for 5 min to allow ions to adsorb onto the surface of the membrane and exposed stirred cell surfaces. 1 mL of the feed solution is taken from the stirred cell and placed in a scintillation vial. The diafiltrate tank is filled with a 100 mM $MgCl_2$ salt solution and ten 7 mL plastic scintillation vials are loaded into the permeate vial holder. After loading the vials, the user inputs the necessary information into the ADD GUI and begins the experiment.

The apparatus works under the assumption that the volumetric flow rate of the diafiltrate entering the stirred cell is equal to the volumetric flow rate of the permeate leaving. To ensure operating conditions that are consistent with this assumption, the diafiltrate tank is not immediately pressurized to the operating pressure as this approach would flood the stirred cell with diafiltrate. Moreover, adding a bolus of high concentration diafiltrate at the onset of the experiment hinders membrane characterization at low concentrations. Instead, the desired operating conditions are created by first increasing the pressure of the whole system to an initial intermediate value. This initial pressure increases the density of gas molecules within the tubing between the diafiltrate tank and stirred cell such that when the pressure is raised to the operating pressure,

https://doi.org/10.1021/acsapm.2c00048
ACS Appl. Polym. Mater. 2022, 4, 3438−3447

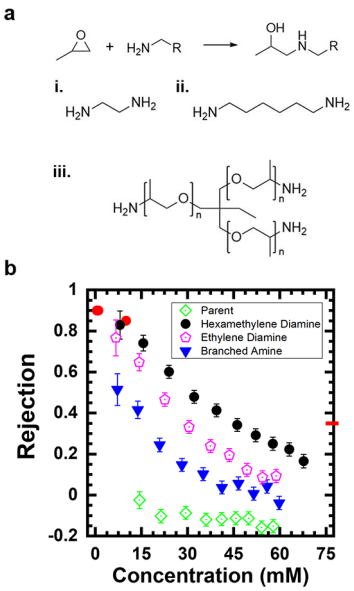

Figure 4. Development of structure function insights for charge-functionalized P(TFEMA−OEGMA−GMA) copolymer membranes is aided by the ADD device. (a) Base-catalyzed epoxide ring opening reaction is used to introduce the desired amine functionality onto the pore walls of parent membranes. The chemical structures of the molecules used to produce charge-functionalized copolymer membranes: (i) ethylene diamine, (ii) hexamethylene diamine, and (iii) trimethylolpropane tris[poly(propylene glycol), amine terminated] ether. (b) Diafiltration experiments with 1 mM $MgCl_2$ feeds and 100 mM $MgCl_2$ diafiltrate solutions are used to probe the concentration-dependent rejection of copolymer membranes. The data for the trimethylolpropane tris[poly(propylene glycol), amine terminated] ether functionalized membranes are denoted as branched amine membranes. The rejections of the functionalized membranes decay to that of the parent polymer membrane at sufficiently high retentate concentrations. The red circles correspond to the rejection values originally reported for the hexamethylene-functionalized copolymer membrane by Qu et al.[18] The red bar corresponds to the rejection reported at 100 mM $MgCl_2$.

the gas compresses into the volume of the headspace and brings the diafiltrate to the entrance of the stirred cell. The transition from the initial to operating pressure is highlighted within the data reported in Figure 3b. The choice of the initial pressure, which is based on the desired operating pressure and the system geometry, is discussed within the Supporting Information. After reaching the operating pressure, the user is free to leave and return at the end of the experiment. As previously discussed, the GUI associated with the ADD device displays the mass, the conductivity of the solution in the stirred cell, and the system pressure throughout the duration of the experiment (Figure 3b). Once the desired mass of permeate is collected, the solenoid valves depressurize the system. Two additional samples are collected: one from the tubing between the stirred cell and the permeate vial and one from the final retentate solution. Both samples are placed in labeled scintillation vials.

Samples from all scintillation vials are prepared for analysis by inductively coupled plasma optical emission spectroscopy (ICP OES). The ICP OES data are imported to MATLAB and analyzed to calculate the solute rejection (Figure 4b), hydraulic permeability (Figure S5a), and solute permeability coefficient (Figure S5b) for each of the vials. A thin film model for mass transfer was used to account for concentration polarization and calculate the concentration at the membrane-feed solution interface, c_{in} (see the Supporting Information for details and equations). Percent rejection was determined using eq 5

$$\%\, R = \left(1 - \frac{c_p}{c_{in}}\right) \times 100 \tag{5}$$

where c_p is the permeate concentration measured by ICP−OES. Figure 4b compares the rejection of the parent membrane (green diamonds) with that of the ethylene diamine (pink pentagons), hexamethylene diamine (black circles), and trimethylolpropane tris[poly(propylene glycol), amine terminated] ether (branched amine, inverted blue triangles) functionalized membranes. The error bars correspond to the systematic and random error associated with each measurement. For each chemistry, experiments with multiple membrane samples are presented in Figure S6. The small sample to sample variation demonstrated in these data sets highlights how the ADD device can help meet the need for reliable data that facilitate the development of new polymer membranes.

After accounting for concentration polarization and osmotic pressure, the hydraulic permeability coefficients were shown to decrease slightly (~25%) with the increase in retentate concentration (Figure S5). The average hydraulic permeability for the hexamethylene-functionalized membrane (2.4 ± 0.5 L m^{-2} h^{-1} bar^{-1}) is 1.6 times higher than the previously reported value (1.5 ± 0.7 L m^{-2} h^{-1} bar^{-1}).[18] This increase in L_p is attributed to a decrease in the thickness of the copolymer film, which results from a modified casting process, not a change in the average pore size.[29]

The agreement between the Mg^{2+} rejection values calculated within this work (Figure 4b, black circles) and the values observed in a prior study (Figure 4b, red circles) provides support for the claim that the increased L_p is a result of the reduced membrane thickness. Solute rejection can be directly related to the solute permeability coefficient, B, and the water flux, J_w (eq 6).

$$\frac{B}{J_w} \sim \frac{B}{L_p \Delta P} = \left(\frac{1 - \%\, R}{\%\, R}\right) \tag{6}$$

For experiments conducted at the same applied pressure, this expression relates B and L_p to % R. B and L_p are both inversely proportional to membrane thickness but exhibit distinct dependencies on pore size. Therefore, the ratio, B/L_p, remains constant with changes in membrane thickness but varies with changes to the nanostructure. The comparable $MgCl_2$ rejection values observed in this and prior efforts are consistent with the ratio B/L_p remaining constant and the membrane nanostructure being unchanged.

The charge-functionalized membranes display distinct concentration-dependent rejection profiles. For all of the amine-functionalized P(TFEMA−OEGMA−GMA) samples, as the concentration of $MgCl_2$ in the retentate increases, rejection decays to that of the uncharged, parent membrane (i.e., approximately zero). A scaling analysis comparing the Debye length to the pore diameter helps rationalize this trend. At low retentate concentrations, the Debye length, λ_D, is greater than the diameter of the pore [e.g., λ_D(2 mM $MgCl_2$) ≅ 4 nm]. Under these conditions, ammonium moieties within the pores are able to effectively repel Mg^{2+} ions, which limits $MgCl_2$ transport. As the retentate concentration increases, the dissolved ions screen the ammonium moieties, decreasing the

https://doi.org/10.1021/acsapm.2c00048
ACS Appl. Polym. Mater. 2022, 4, 3438−3447

Debye length. At sufficiently high concentrations, the Debye length is comparable to the pore size [e.g., λ_D(40 mM $MgCl_2$) ≅ 0.9 nm] and the ammonium moieties cannot regulate Mg^{2+} transport as effectively. This rationale holds true for all of the charge-functionalized membranes. Between the three amine chemistries, however, there are differences in the variation of rejection, which the diafiltration experiments are capable of elucidating, that cannot be explained using this scaling analysis. For instance, the hexamethylene diamine membrane rejects $MgCl_2$ to a greater extent than the ethylene diamine material. This observation suggests that distributing the charge toward the center of a pore, by increasing the length of the spacer between the terminal ammonium and the pore wall, may be an effective molecular design strategy for enhancing ion rejection. The low rejection values observed for the branched amine supports this hypothesis. In this case, the low solubility of the poly(propylene glycol) spacer causes it to collapse toward the pore wall and limits its ability of spread charge into the pore. The distinct rejection profiles suggest that Debye screening arguments alone are not sufficient to describe the influence of the spacer length and chemistry on membrane performance. Instead, the influence of these pore wall modifications on the membrane nanostructure (e.g., charge density, crosslinking, and swelling) must also be taken into account. Without the full rejection profiles, it would be impossible to elucidate the mechanisms that impact selective solute transport.

Ultimately, the diafiltration experiments with the ADD device are able to provide a fuller picture of membrane performance as the system transitions from low and high concentration regimes. This approach improves on previous techniques that require multiple filtration experiments to characterize membrane performance under varying feed conditions.[18,29,31] In total, the ADD device characterizes membranes ∼40% faster than a previously reported diafiltration apparatus (Table 1).[17] When compared to traditional filtration campaigns, the total improvement in time saved is ∼90%.

Because the ADD device continuously monitors the retentate concentration during diafiltration experiments, it can provide insights into the solute removal mechanism. Specifically, the solute can be rejected by the membrane or removed through adsorptive processes. While both mechanisms lead to decreased analyte concentrations in the permeate, information on the retentate is necessary to distinguish between rejection and adsorption. Polymer membranes that reject solutes retain them in the retentate, which leads to an increase in the retentate concentration as the experiment progresses. Conversely, adsorptive processes sequester the solute from solution such that the retentate concentration does not change or decreases. Therefore, the retentate concentration profile can be used to elucidate the mechanisms through which solutes are removed. Within this work, the increase in retentate concentration is consistent with the rejection of $MgCl_2$. These rejections are calculated using measurements from the inline conductivity probe which are confirmed by conducting mass balance calculations that are outlined in detail within the Supporting Information. Distinguishing between the two mechanisms is particularly important for the development and implementation of polymer membranes with solute tailored selectivity.[20]

Table 1. Comparison Highlights the Benefits of Automating the Diafiltration Apparatus[a]

	before	after
experimental setup (min)	25	25
experimental operating time (min)	108	2
membrane rinse/wash (min)	45	45
data analysis (ICP OES) prep (min)	30	30
ICP OES run time (min)	114	114
manual analysis (min)	60	5
total time (min)	382	221
time saved with the ADD device (min)	161	
time saved with the ADD device (percent)	42%	

[a]Within a given experiment, 10 permeate samples are collected with 1 g of permeate in each vial. The motor removes the need for an experimenter to be present. As data are consistently recorded from one experiment to the next, the post processing capabilities of the ADD device removes the need for users to independently import and process data. These automated experiments require ∼40% less time to characterize membranes than the previously reported diafiltration apparatus.

3.4. Versatile Software Permits the Characterization of Absorbent Membranes. The versatility of the ADD device is evidenced by the alternate experimental configuration, shown in Figure 5, which was used to quantify the solute capture characteristics of a membrane sorbent. Membrane sorbents possess pore walls lined by selective ligands that bind analytes to remove them from the effluent solution. Because diffusion to the ligands occurs over short length scales commensurate with the pore diameter, mass transfer in membrane sorbents is rapid and often controlled by convection. The efficient solute capture that results from these conditions has been used to remove organic pollutants[32] and heavy metals[33] from water, as well as to identify the protein targets of small molecule drugs.[34] Figure 5a shows a modified apparatus for the execution of a constant volumetric flux breakthrough experiment. The stirred cell and diafiltration tank are replaced by a membrane holder and syringe pump. The tubing for the permeate collection is kept the same. This experiment uses the ability of the ADD device to automatically collect and switch permeate vials. Mass data are recorded and displayed in a manner analogous to that of diafiltration experiments.

Within a breakthrough experiment, the effluent permeate concentration is monitored as a function of volume permeated to provide data on the removal of a target solute. In the initial intervals, a large portion of the target solute is captured, as there is a high density of binding sites available. Therefore, the permeate concentration should remain near zero. As a larger fraction of the sites become occupied, more solute can permeate through the membrane without being captured, leading to the concentration in the permeate rising (i.e., the solute breaking through). In addition to the quantifying sorbent capacity, breakthrough experiments can shed light on the efficiency of the separation and the dispersity in the pore size.[35] A sharp breakthrough curve indicates a uniform pore distribution and, compared to the diffusion time to the active sites, a long residence time within the membrane.[35] To conduct breakthrough experiments, several changes occur within the GUI setup. To begin, the "Experiment Type" setting will be changed from "Diafiltration" to "Permeability/Breakthrough", and because the system does not use a pressure transducer or conductivity probe, the experimenter can select to not record pressure and conductivity data. Once again, the experimenter can specify the amount of permeate collected

https://doi.org/10.1021/acsapm.2c00048
ACS Appl. Polym. Mater. 2022, 4, 3438−3447

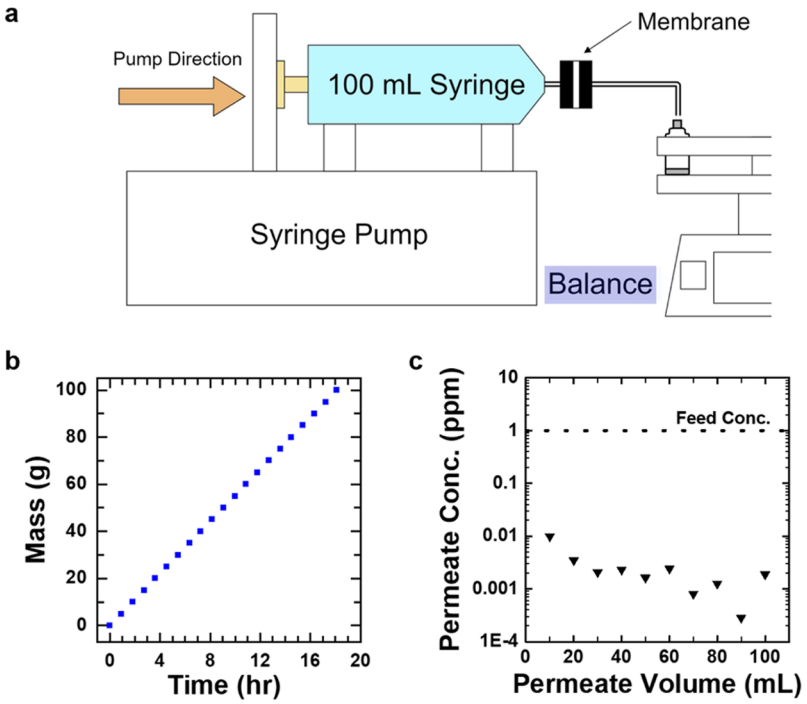

Figure 5. (a) Apparatus is adapted for constant volumetric breakthrough experiments. The syringe contains a low concentration solute (e.g., $CuCl_2$) that permeates through a stack of three PEI functionalized membranes. Ten aliquots of permeate are collected at 10 mL intervals in scintillation vials. (b) Mass data are collected throughout the experiment. (c) Post processed ICP OES data present the concentration of $CuCl_2$ (ppm) in each permeate vial. The dashed line represents the initial feed concentration of 1 ppm $CuCl_2$.

within each vial. For longer experiments, the glass scintillation vials, which hold up to 20 mL of solution, are used. The "Pre and Post Experiment Notes" text boxes provide the experimenter an opportunity to record the settings programmed in the syringe pump as well as the initial feed concentration and identity of the solute of interest.

A model Cu^{2+} breakthrough experiment was conducted with a branched polyethyleneimine (PEI)-functionalized membrane sorbent.[33] Three membranes were cut into 1 cm diameter circles and stacked on top of one another within a filter holder. The syringe pump was loaded with a 1 ppm $CuCl_2$ feed solution. An aliquot of this solution was stored within a separate scintillation vial for subsequent analysis. The GUI was set to collect 10 vials of permeate, each containing 10 mL of solution. The syringe pump flow rate was set to 0.092 mL min^{-1}. The resulting mass versus time data (Figure 5b) increases linearly, which is consistent with the constant volumetric flow rate. Furthermore, the slope of the line confirms the flow rate of the syringe pump. At the end of the experiment, the permeate vials were collected and analyzed using ICP−OES. The dashed line within Figure 5c corresponds to the 1 ppm $CuCl_2$ feed solution that was loaded within the syringe. The inverted triangles correspond to the concentration of $CuCl_2$ within each of the permeate vials. The data are consistent with the previously reported 99% removal of heavy metal ions. Visual inspection of the membrane surface following the experiment revealed its color had changed from white to blue, which is consistent with the effective capture and removal of Cu^{2+} ions. However, due to the high capacity and efficient mass transfer of the PEI-functionalized sorbents, Cu^{2+} breakthrough is not observed due to the limited feed solution volume that could be held by the syringe pump. An experiment using a higher initial feed concentration or a larger volume of solution would be necessary to see the Cu^{2+} breakthrough with this membrane system. Nonetheless, the flexibility of the ADD device is highlighted.

4. CONCLUSIONS

Functional polymers are a promising route toward the development of membranes with selectivities tailored for several important applications. Advancing these materials will require rigorous analysis and understanding of fluxes as a function of operating conditions. Within this study, commercially available hardware in conjunction with 3D-printed parts and an in-house MATLAB program automated the collection of permeate mass, retentate conductivity, and pressure data. The consistency of the data formatting allows an additional MATLAB code to conduct all post experimental data analysis. Compared to previous methods, automated experiments reduce the time necessary to conduct conventional diafiltration experiments by 40%. The ADD device was able to replicate experimental data for a hexamethylene diamine-functionalized P(TFEMA−OEGMA−GMA) membrane that rejects dissolved salts through co-ion exclusion. Using the device, the membrane properties were characterized over a wide range of conditions that bridged the gap between experiments at low and high solute concentrations, thereby providing a better representation of the concentration-dependent parameters (e.g., permeability coefficients and solute rejection) in one experiment. Furthermore, this approach was leveraged to elucidate nuanced differences in the variation of $MgCl_2$ rejection with concentration, which may have been overlooked if experiments at only low and high concentrations were explored. As such, the versatile ADD device has the potential to assist in the generation of structure−function insights that can guide the design of polymer membranes.

https://doi.org/10.1021/acsapm.2c00048
ACS Appl. Polym. Mater. 2022, 4, 3438−3447

■ ASSOCIATED CONTENT

Supporting Information

The Supporting Information is available free of charge at https://pubs.acs.org/doi/10.1021/acsapm.2c00048.

Conductivity board modifications, conductivity probe lead preparation and stirred cell placement, calibration curve for $MgCl_2$ quantification, permeate vial holder image, conductivity and pressure readings for overflow and lag experiments, concentration versus hydraulic permeability for four functionalities, concentration versus solute permeability for four functionalities, duplicate rejection versus concentration plots, maximum permeate flow rate calculations, evaporative permeate losses derivation, GUI discussion and operating considerations, constant volume stirred cell mass balances, and variable volume stirred cell mass balances (PDF)

■ AUTHOR INFORMATION

Corresponding Author

William A. Phillip − *Department of Chemical and Biomolecular Engineering, University of Notre Dame, Notre Dame, Indiana 46556, United States;* orcid.org/0000-0001-8871-585X; Email: wphillip@nd.edu

Authors

Zachary W. Muetzel − *Department of Chemical and Biomolecular Engineering, University of Notre Dame, Notre Dame, Indiana 46556, United States*

Jonathan Aubuchon Ouimet − *Department of Chemical and Biomolecular Engineering, University of Notre Dame, Notre Dame, Indiana 46556, United States*

Complete contact information is available at: https://pubs.acs.org/10.1021/acsapm.2c00048

Notes

The authors declare no competing financial interest.

■ ACKNOWLEDGMENTS

This work was made possible with support from the National Science Foundation (NSF) through the Advanced Manufacturing Program (award number: 1932206), and we appreciatively acknowledge this support. We would like to thank the Center for Environmental Science and Technology at the University of Notre Dame (CEST) portions of this research was performed with instruments at this facility. Z.W.M. gratefully acknowledges support for this project from the Vincent P. Slatt Fellowship for Undergraduate Research in Energy Systems and Processes, administered by the Center for Sustainable Energy at Notre Dame.

■ REFERENCES

(1) Daufin, G.; Escudier, J.-P.; Carrère, H.; Bérot, S.; Fillaudeau, L.; Decloux, M. Recent and Emerging Applications of Membrane Processes in the Food and Dairy Industry. *Food Bioprod. Process.* **2001**, *79*, 89−102.

(2) Zydney, A. L. New Developments in Membranes for Bioprocessing − A Review. *J. Membr. Sci.* **2021**, *620*, 118804.

(3) Jabra, M. G.; Yehl, C. J.; Zydney, A. L. Multistage Continuous Countercurrent Diafiltration for Formulation of Monoclonal Antibodies. *Biotechnol. Prog.* **2019**, *35*, No. e2810.

(4) Nambiar, A. M. K.; Li, Y.; Zydney, A. L. Countercurrent Staged Diafiltration for Formulation of High Value Proteins. *Biotechnol. Bioeng.* **2018**, *115*, 139−144.

(5) Shao, J.; Zydney, A. L. Optimization of Ultrafiltration/Diafiltration Processes for Partially Bound Impurities. *Biotechnol. Bioeng.* **2004**, *87*, 286.

(6) Ghosh, R.; Chen, G.; Roshankhah, R.; Umatheva, U.; Gatt, P. A Z2 Laterally-Fed Membrane Chromatography Device for Fast High-Resolution Purification of Biopharmaceuticals. *J. Chromatogr. A* **2020**, *1629*, 461453.

(7) Qiu, X.; Yu, H.; Karunakaran, M.; Pradeep, N.; Nunes, S. P.; Peinemann, K. V. Selective Separation of Similarly Sized Proteins with Tunable Nanoporous Block Copolymer Membranes. *ACS Nano* **2013**, *7*, 768.

(8) Corrado, T.; Guo, R. Macromolecular Design Strategies toward Tailoring Free Volume in Glassy Polymers for High Performance Gas Separation Membranes. *Mol. Syst. Des. Eng.* **2020**, *5*, 22−48.

(9) Corrado, T.; Huang, Z.; Aboki, J.; Guo, R. Microporous Polysulfones with Enhanced Separation Performance via Integration of the Triptycene Moiety. *Ind. Eng. Chem. Res.* **2020**, *59*, 5351−5361.

(10) Freeman, B. D. Basis of Permeability/Selectivity Tradeoff Relations in Polymeric Gas Separation Membranes. *Macromolecules* **1999**, *32*, 375−380.

(11) Zhang, Y.; Almodovar-Arbelo, N. E.; Weidman, J. L.; Corti, D. S.; Boudouris, B. W.; Phillip, W. A. Fit-for-Purpose Block Polymer Membranes Molecularly Engineered for Water Treatment. *npj Clean Water* **2018**, *1*, 2.

(12) Weidman, J. L.; Mulvenna, R. A.; Boudouris, B. W.; Phillip, W. A. Nanoporous Block Polymer Thin Films Functionalized with Bio-Inspired Ligands for the Efficient Capture of Heavy Metal Ions from Water. *ACS Appl. Mater. Interfaces* **2017**, *9*, 19152−19160.

(13) van Reis, R.; Zydney, A. Bioprocess Membrane Technology. *J. Membr. Sci.* **2007**, *297*, 16−50.

(14) Werber, J. R.; Osuji, C. O.; Elimelech, M. Materials for Next-Generation Desalination and Water Purification Membranes | Nature Reviews Materials. *Nat. Rev. Mater.* **2016**, *1*, 16018.

(15) Cussler, E. L. *Diffusion: Mass Transfer in Fluid Systems*; Cambridge University Press, 2009.

(16) Kedem, O.; Katchalsky, A. Thermodynamic Analysis of the Permeability of Biological Membranes to Non-Electrolytes. *Biochim. Biophys. Acta* **1958**, *27*, 229−246.

(17) Ouimet, J. A.; Liu, X.; Brown, D. J.; Eugene, E. A.; Popps, T.; Muetzel, Z. W.; Dowling, A. W.; Phillip, W. A. DATA: Diafiltration Apparatus for High-Throughput Analysis. *J. Membr. Sci.* **2021**, *641*, 119743.

(18) Qu, S.; Dilenschneider, T.; Phillip, W. A. Preparation of Chemically-Tailored Copolymer Membranes with Tunable Ion Transport Properties. *ACS Appl. Mater. Interfaces* **2015**, *7*, 19746−19754.

(19) Kamcev, J.; Paul, D. R.; Manning, G. S.; Freeman, B. D. Predicting Salt Permeability Coefficients in Highly Swollen, Highly Charged Ion Exchange Membranes. *ACS Appl. Mater. Interfaces* **2017**, *9*, 4044−4056.

(20) Sujanani, R.; Landsman, M. R.; Jiao, S.; Moon, J. D.; Shell, M. S.; Lawler, D. F.; Katz, L. E.; Freeman, B. D. Designing Solute-Tailored Selectivity in Membranes: Perspectives for Water Reuse and Resource Recovery. *ACS Macro Lett.* **2020**, *9*, 1709−1717.

(21) Ghosh, R.; Wan, Y.; Cui, Z.; Hale, G. Parameter Scanning Ultrafiltration: Rapid Optimisation of Protein Separation. *Biotechnol. Bioeng.* **2003**, *81*, 673−682.

(22) Ghosh, R.; Cui, Z. Analysis of Protein Transport and Polarization through Membranes Using Pulsed Sample Injection Technique. *J. Membr. Sci.* **2000**, *175*, 75−84.

(23) Sadeghi, I.; Asatekin, A. Membranes with Functionalized Nanopores for Aromaticity-Based Separation of Small Molecules. *ACS Appl. Mater. Interfaces* **2019**, *11*, 12854−12862.

(24) Yaroshchuk, A.; Bruening, M. L. An Analytical Solution of the Solution-Diffusion-Electromigration Equations Reproduces Trends in

Ion Rejections during Nanofiltration of Mixed Electrolytes. *J. Membr. Sci.* **2017**, *523*, 361−372.
(25) Cheng, C.; Yaroshchuk, A.; Bruening, M. L. Fundamentals of Selective Ion Transport through Multilayer Polyelectrolyte Membranes. *Langmuir* **2013**, *29*, 1885−1892.
(26) Li, C.; Ramasamy, D. L.; Sillanpää, M.; Repo, E. Separation and Concentration of Rare Earth Elements from Wastewater Using Electrodialysis Technology. *Sep. Purif. Technol.* **2021**, *254*, 117442.
(27) Yang, Z.; Fang, W.; Wang, Z.; Zhang, R.; Zhu, Y.; Jin, J. Dual-Skin Layer Nanofiltration Membranes for Highly Selective Li+/Mg2+ Separation. *J. Membr. Sci.* **2021**, *620*, 118862.
(28) Wang, L.; Rehman, D.; Sun, P.-F.; Deshmukh, A.; Zhang, L.; Han, Q.; Yang, Z.; Wang, Z.; Park, H.-D.; Lienhard, J. H.; Tang, C. Y. Novel Positively Charged Metal-Coordinated Nanofiltration Membrane for Lithium Recovery. *ACS Appl. Mater. Interfaces* **2021**, *13*, 16906−16915.
(29) Dugas, M. P.; Every, G. V.; Park, B.; Hoffman, J. R.; LaRue, R. J.; Bush, A. M.; Zhang, Y.; Schaefer, J. L.; Latulippe, D. R.; Phillip, W. A. Resilient Hollow Fiber Nanofiltration Membranes Fabricated from Crosslinkable Phase-Separated Copolymers. *Mol. Syst. Des. Eng.* **2020**, *5*, 943−953.
(30) Hoffman, J. R.; Phillip, W. A. Dual-Functional Nanofiltration Membranes Exhibit Multifaceted Ion Rejection and Antifouling Performance. *ACS Appl. Mater. Interfaces* **2020**, *12*, 19944−19954.
(31) Zhang, Y.; Mulvenna, R. A.; Qu, S.; Boudouris, B. W.; Phillip, W. A. Block Polymer Membranes Functionalized with Nanoconfined Polyelectrolyte Brushes Achieve Sub-Nanometer Selectivity. *ACS Macro Lett.* **2017**, *6*, 726−732.
(32) Wang, Z.; Cui, F.; Pan, Y.; Hou, L.; Zhang, B.; Li, Y.; Zhu, L. Hierarchically Micro-Mesoporous *β*-Cyclodextrin Polymers Used for Ultrafast Removal of Micropollutants from Water. *Carbohydr. Polym.* **2019**, *213*, 352−360.
(33) Zhang, Y.; Vallin, J. R.; Sahoo, J. K.; Gao, F.; Boudouris, B. W.; Webber, M. J.; Phillip, W. A. High-Affinity Detection and Capture of Heavy Metal Contaminants Using Block Polymer Composite Membranes | ACS Central Science. *ACS Cent. Sci.* **2018**, *4*, 1697−1707.
(34) Yang, L.; Bui, L.; Hanjaya-Putra, D.; Bruening, M. L. Membrane-Based Affinity Purification to Identify Target Proteins of a Small-Molecule Drug. *Anal. Chem.* **2020**, *92*, 11912−11920.
(35) Weidman, J. L.; Mulvenna, R. A.; Boudouris, B. W.; Phillip, W. A. Nanostructured Membranes from Triblock Polymer Precursors as High Capacity Copper Adsorbents. *Langmuir* **2015**, *31*, 11113−11123.

https://doi.org/10.1021/acsapm.2c00048
ACS Appl. Polym. Mater. 2022, 4, 3438−3447